Urea-Modified Carbon Nitrides: Enhancing Photocatalytic Hydrogen Evolution by Rational Defect Engineering

*Vincent Wing-hei Lau, Victor Wen-zhe Yu, Florian Ehrat, Tiago Botari, Igor Moudrakovski, Thomas Simon, Viola Duppel, Elise Medina, Jacek K. Stolarczyk, Jochen Feldmann, Volker Blum, and Bettina V. Lotsch**

The primary amine groups on the heptazine-based polymer melon, also known as graphitic carbon nitride (g-C_3N_4), can be replaced by urea groups using a two-step postsynthetic functionalization. Under simulated sunlight and optimum Pt loading, this urea-functionalized carbon nitride has one of the highest activities among organic and polymeric photocatalysts for hydrogen evolution with methanol as sacrificial donor, reaching an apparent quantum efficiency of 18% and nearly 30 times the hydrogen evolution rate compared to the nonfunctionalized counterpart. In the absence of Pt, the urea-derivatized material evolves hydrogen at a rate over four times that of the nonfunctionalized one. Since "defects" are conventionally accepted to be the active sites in graphitic carbon nitride for photocatalysis, the work here is a demonstrated example of "defect engineering," where the catalytically relevant defect is inserted rationally for improving the intrinsic, rather than extrinsic, photocatalytic performance. Furthermore, the work provides a retrodictive explanation for the general observation that g-C_3N_4 prepared from urea performs better than those prepared from dicyandiamide and melamine. In-depth analyses of the spent photocatalysts and computational modeling suggest that inserting the urea group causes a metal-support interaction with the Pt cocatalyst, thus facilitating interfacial charge transfer to the hydrogen evolving centers.

1. Introduction

Photocatalytic hydrogen evolution from water provides a direct method to capture and store sunlight as chemical energy, which can then be released in an environmentally friendly energy cycle. While a large library of photocatalytic materials has been catalogued[1] in the four decades since Honda's and Fujishima's report on photocatalytic water-splitting by TiO_2,[2] one of the most promising photocatalysts is the heptazine-based graphitic carbon nitride (g-C_3N_4), historically known since Liebig's era as melon.[3] Melon is a 1D polymer of heptazine, bridged by secondary amines, with neighboring polymer strands hydrogen-bonded together into quasi 2D arrays that form stacks through π–π interaction (**Scheme 1**, left).[4] Graphitic carbon nitride has also been depicted in the literature as a fully condensed 2D layered structure with tertiary amines bridging every heptazine unit (Scheme 1, middle),[5] although this fully condensed material has not been unambiguously shown to form experimentally to date. In 2009, the related yet fully 2D linked framework, poly(heptazine imide) or PHI, was reported (Scheme 1, right). PHI has a hexagonal network where each heptazine forms three secondary amine bonds with neighboring heptazine units.[6]

Graphitic carbon nitride as a photocatalyst has the advantages of being easily prepared from inexpensive precursors (melamine, dicyandiamide, or urea),[7] having appropriate energy levels straddling the redox potential required for water splitting,[8] functioning under visible light irradiation, and being chemically stable. Overcoming one of its major disadvantages—its activity is still very moderate—is the subject of research in numerous reports on carbon nitride photocatalysis. Most of the publications on graphitic carbon nitride thus far focus on three main strategies for activity enhancement: (1) redshifting the absorption onset through copolymerization with dopant(s),[9] (2) texturization for surface area increase,[10] and (3) composite formation with a (semi)conductor for improving photoexcited charge separation.[11] While useful, there is a striking lack of attempts to enhance the intrinsic activity of carbon nitrides, which is aggravated by the limited molecular tunability of carbon nitrides due to their insolubility and lack of reactivity.

Dr. V. W.-h. Lau, Dr. I. Moudrakovski, V. Duppel, E. Medina, Prof. B. V. Lotsch
Max Planck Institute for Solid State Research
Heisenbergstraße 1, 70569 Stuttgart, Germany
E-mail: b.lotsch@fkf.mpg.de

V. W.-z. Yu, Dr. T. Botari, Prof. V. Blum
Department of Mechanical Engineering and Materials Science
Duke University
Durham, NC 27708, USA

F. Ehrat, T. Simon, Dr. J. K. Stolarczyk, Prof. J. Feldmann
Photonics and Optoelectronics Group
Department of Physics and Center for Nanoscience (CeNS)
Ludwig-Maximilians-Universität (LMU)
Amalienstraße 54, 80799 Munich, Germany

F. Ehrat, T. Simon, Dr. J. K. Stolarczyk, Prof. J. Feldmann, Prof. B. V. Lotsch
Nanosystems Initiative Munich (NIM)
Schellingstraße 4, 80799 Munich, Germany

Prof. B. V. Lotsch
Department of Chemistry
University of Munich
Butenandtstraße 5-13, 81377 Munich, Germany

DOI: 10.1002/aenm.201602251

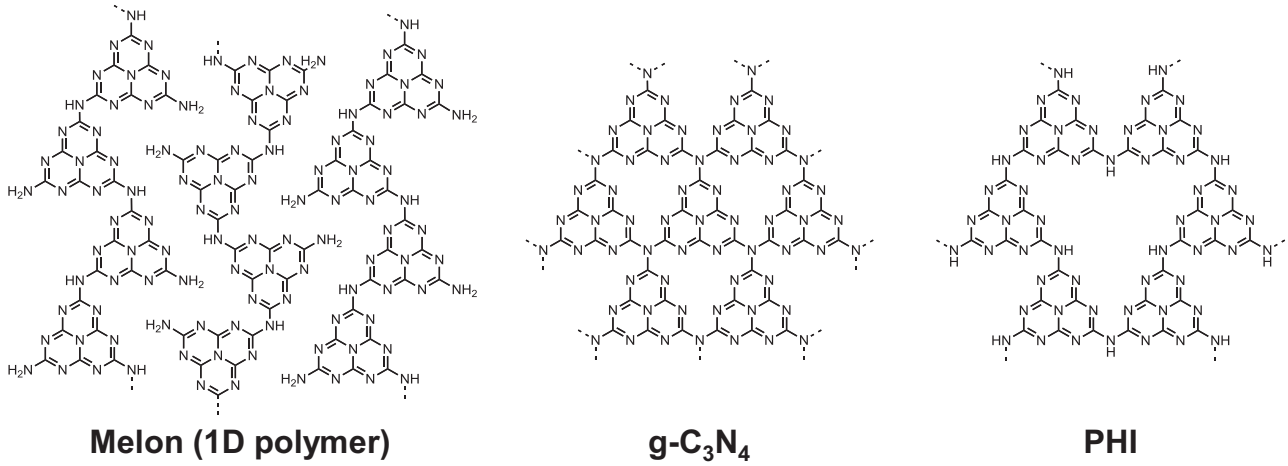

Scheme 1. Structures of "graphitic carbon nitrides." Shown are the 1D polymer melon (left), the fully condensed 2D counterpart (middle), and the 2D network PHI.

Here, the terms intrinsic and extrinsic with respect to the catalytic properties are differentiated based on the definition proposed by Vojvodic and Nørskov: intrinsic refers to the chemical composition and structure of the catalyst material, whereas extrinsic refers to either geometrical structuring (strategy 2) and/or its interface with another solid material, liquid or gas to influence the host catalyst (strategy 3).[12] At the same time, improving the interfacial transfer of photoexcited charges to the reactants—via the cocatalyst—constitutes an important yet somewhat overlooked strategy for improving photocatalytic activity.[13] Even in the very efficient CdSe-Pt system, it is estimated that only 40% of the photoexcited electrons are transferred to the platinum from spherical CdSe particles,[14] a prerequisite step for hydrogen evolution. We and others have shown that the carbon nitride photocatalysts can function with a range of hydrogen evolving electrocatalysts that are synthetic, biological, or bioinspired, with activity rivaling that of platinum,[15] even though the coupling between these catalysts and the polymer is rather weak.[15e] To address this, we have investigated the structural features that lead to photocatalytic activity in amorphous melon as opposed to crystalline melon, which exhibits negligible activity.[16] Unlike crystalline melon, which is prepared in a sealed ampoule under autogeneous ammonia pressure leading to reversible reaction conditions and crystal defect healing, we have previously shown[17] that amorphous melon contains crystal imperfections in the form of dangling moieties resulting from incomplete cyclization and polymerization, or impurities (e.g., oxygen) from the precursor. Using the methodology of model photocatalysts, we identified the functional groups that may be considered as the "defects" responsible for photocatalytic activity, namely the cyanamide moiety ($-NCN^-$) and oxygen-bearing functional groups ($-O^-$, $-OH$, $-COOH$), which can be present due to incomplete cyclization of the heptazine or incorporation of oxygen from the atmosphere or precursor.

Using this knowledge, we were furthermore able to demonstrate the concept of active site engineering for activity improvement, that is, the rational insertion of the catalytically relevant "defect" into the heptazine structure. This concept was illustrated by converting the primary amines of melon into anionic cyanamides, one of the "defects" identified, through a postsynthetic treatment with KSCN to yield a material (henceforth notated as NCN-CN_x; see **Scheme 2**) outperforming melon by over 12 times at optimum Pt loading.[17]

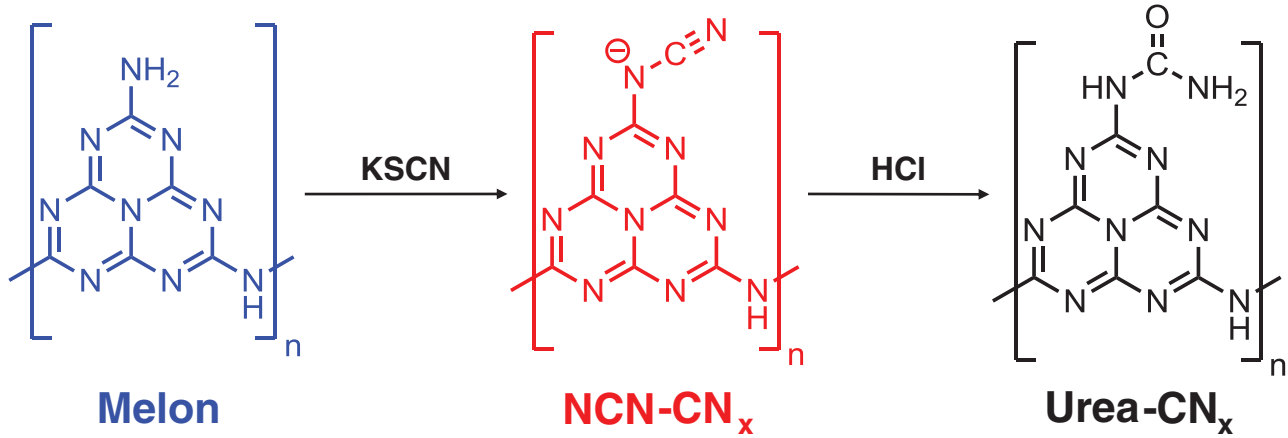

Scheme 2. Simplified reaction scheme of the compound synthesized in this work, showing melon and its conversion to NCN-CN_x by a postsynthetic reaction using KSCN melt, and its acid-induced hydrolysis to urea-CN_x.

Note that, in Scheme 2, we have depicted only the site where the incorporated functional group is present, which is either at every heptazine unit assuming a 1D polymeric heptazine backbone or at the periphery of the 2D network array of PHI (Scheme S1, Supporting Information). The roles of such "defects" may be to: (1) act as the reduction or oxidation reaction sites,[18] (2) facilitate intermolecular interactions to improve overall reaction kinetics through increased catalyst-substrate affinity,[15f] (3) modify energy levels or carrier dynamics,[17] and/or (4) enable strong photocatalyst/cocatalyst interactions to facilitate charge transfer.[17]

As the cyanamide group can be hydrolyzed to urea,[19] we here exploit this synthetic procedure to introduce an oxygen-containing group into the heptazine polymer, since our previous work identified oxy- or carboxylate as groups potentially relevant for photocatalysis.[17] The obvious advantage of this route is that, unlike heating the precursor in oxygen or incorporating a dopant stochastically into the polymer, an oxygen-containing moiety such as urea can be controllably inserted at the peripheral sites of the heptazine units, thus facilitating characterization of the polymer for elucidating structure–activity relationship. As will be shown here, this hydrolysis product—notated as urea-CN_x—exhibits photocatalytic activity for hydrogen evolution outperforming even that of NCN-CN_x and melon despite absorbing less in the visible region. The role of the urea moiety is rationalized based on experimental and computational findings. Lastly, we provide a retrodictive explanation of why melon has higher activity when synthesized from urea compared to dicyandiamide or melamine[20] based on the structural characterization of urea-CN_x. This finding has particular importance given that a number of carbon nitride systems capable of complete water splitting employed melon prepared from urea, while those prepared from other precursors (e.g., dicyandiamide) exhibited low water-splitting activity.[21] Hence, the results herein highlight the implications of the approach of "defect engineering" for systematically improving carbon nitride photocatalysts.

2. Results and Discussions

Since strong acids are known to catalyze the hydrolysis of cyanamides to form urea,[19a] the NCN-CN_x (experimental details in the Supporting Information) is assumed to undergo hydrolysis at the cyanamide sites specifically when treated with HCl. This acid-treated material, which we tentatively notate henceforth as urea-CN_x, was evaluated for photocatalytic hydrogen evolution under simulated sunlight (AM1.5) under a range of conditions, as shown in **Figure 1**. At the optimized Pt loading of 2 wt%, deposited in situ by the photoreduction of H_2PtCl_6, and using methanol (10 vol%) as the electron donor, the urea-CN_x (20 mg) exhibited a stable hydrogen evolution rate of 56.2 μmol h^{-1} for over 100 h of irradiation, more than twice the stable rate of NCN-CN_x (24.7 μmol h^{-1}, optimized at 8 wt% Pt) and almost 30 times that of melon (2.0 μmol h^{-1}, optimized at 1 wt% Pt). In terms of apparent quantum efficiency (AQE) at 400 nm, urea-CN_x has a value of 17.9%, nearly double that of NCN-CN_x at 9.3% and nearly 36 times higher than that of melon at 0.5%. These performance metrics are summarized in Table S3 (Supporting Information); the action spectra of the three catalysts are shown in **Figure 2**b. Though caution must be exercised when comparing literature results,[22] the urea-CN_x here exhibits one of the highest activities for the sacrificial hydrogen evolution half reaction amongst organic and polymeric visible-light photocatalysts (comparison with literature values given in Table S4, Supporting Information) both in relative terms (i.e., outperformance over a photocatalyst standard) as an IUPAC recommendation,[23] or in absolute terms using quantum efficiency as the performance metric as suggested by researchers in the field.[24] Note that higher quantum yields are generally obtained when triethanolamine is used due to its more reductive potential, current doubling and other effects;[25] we nonetheless did not select this electron donor for activity benchmarking as it is light sensitive, often contains optical impurities, and has a complex photo-oxidation mechanism involving many intermediates,[26] as compared to the well-studied, clean photo-oxidation of methanol.[27] Furthermore, we have also observed that a number of photocatalysts exhibiting high activity with triethanolamine perform poorly with other electron donors such as methanol (Table S4, Supporting Information).

The urea-CN_x can evolve hydrogen photocatalytically using a range of different electron donors (Figure 1c); in the absence of electron donor, trace amounts of hydrogen were detected after over 12 h, albeit just over the detection limit of our GC. More significantly, urea-CN_x evolved hydrogen photocatalytically even without the addition of Pt cocatalyst (Figure 1d), with an average rate in the first 24 h of 17 nmol h^{-1}, over four times that of NCN-CN_x (4.2 nmol h^{-1}) and melon (3.5 nmol h^{-1}). The apparent correlation between the BET (Brunauer-Emmett-Teller) surface area and hydrogen evolution rate of urea-CN_x and melon suggests that surface area is one key determinant for activity in the Pt-free case. Insertion of Pt cocatalyst, however, changes the contribution of this factor substantially, as the surface area no longer sufficiently accounts for the high activity of urea-CN_x. Based on the comparison of the hydrogen evolution rate at optimized Pt loading normalized to the BET surface area, urea-CN_x evolves hydrogen at a rate of 43.5 μmol h^{-1} m^{-2}, far outperforming NCN-CN_x at 22.5 μmol h^{-1} m^{-2} and melon at 6.1 μmol h^{-1} m^{-2}, as summarized in Table S3 (Supporting Information). Notably, the superior photocatalytic activity of urea-CN_x cannot be attributed to increased light collection since, as the action spectra in Figure 2b show, it has an absorption onset of around 435 nm, which is blueshifted by 25 nm (0.15 eV) from that of melon and NCN-CN_x, both with onset at 460 nm. Rather, urea-CN_x is utilizing the fewer absorbed photons far more efficiently for the desired redox reaction than the other two samples, given that the solar irradiance peaks at around 500 nm. Collectively, these observations point toward an intrinsic improvement in photocatalytic performance which, as shown below, is attributable to the structural features of urea-CN_x and their role in the photocatalytic reaction.

Urea-CN_x was characterized by spectroscopic methods and the results are shown in Figure 2. All solid-state ^{13}C and ^{15}N NMR experiments (Figure 2c,d, respectively) were performed using the sample prepared from isotope-enriched $KS^{13}C^{15}N$, with the enriched samples showing identical FTIR spectra except for the isotope shifts (Figure S3, Supporting Information), and compared against ^{13}C and ^{15}N enriched

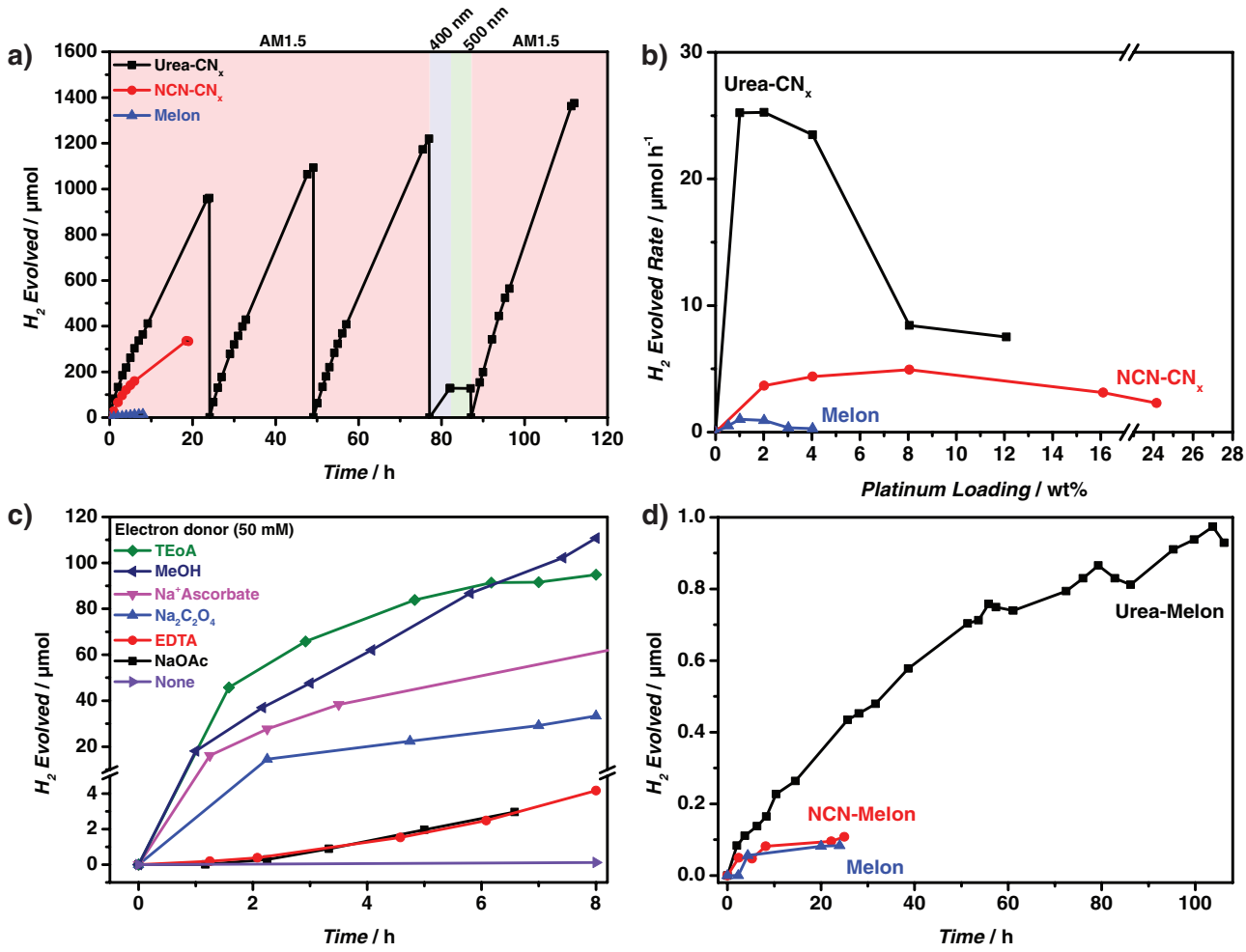

Figure 1. a) Photocatalytic hydrogen evolution under AM1.5, 400 or 500 nm band pass irradiation using methanol (10 vol%) as electron donor at the optimized Pt loading. Reactor headspace was purged after every overnight cycle, and methanol (200 µL) was added on the 24th and 87th hour. Since the gas chromatograph (GC) is operated manually, sampling is done at irregular intervals giving the illusion that the rate is increasing. b) Optimization of hydrogen evolution rate to Pt loading. c) Hydrogen evolution under AM1.5 irradiation and optimized Pt loading using different electron donors (50×10^{-3} M); note that the nonlinearity of some plots is due to the break in the *y*-axis. d) Photocatalytic hydrogen evolution without Pt cocatalyst under AM1.5 irradiation, using aqueous methanol as electron donor (10 vol%); note that some plots appear erratic as the amounts of hydrogen evolved were small and may be affected by frequent sampling.

urea. Urea-CN_x retained its heptazine character, as evidenced by the ring-sextant out-of-plane bending vibration in the IR (809 cm^{-1}), the signals associated with the central (–217.6 ppm) and outer heptazine nitrogen atoms (N1: –175.2 ppm) in the ^{15}N NMR spectra as well as the inner (C2: 158.2 ppm) and outer (C1: 164.1 ppm) carbon atoms in the ^{13}C NMR spectra.[28] The characteristic signals for the 2° amine bridging the heptazine units are observable in the IR (1308 and 1212 cm^{-1})[29] and in the ^{15}N spectra (N3: –240 ppm), while the absence of a ^{15}N signal at –265 ppm indicates the complete conversion of the melon primary amine into cyanamide in the first step of Scheme 2.[3a] The presence of the urea group can be identified by its characteristic FTIR signals at 1653, 1579, and 1549 cm^{-1}, the carbonyl signal (C3) at ≈166 ppm as a signal tail to signal C1, and the urea $-NH_2$ signal (N4) at –290 ppm. Compared to urea, the ^{13}C and ^{15}N chemical shifts of urea-CN_x are slightly shifted downfield, which we attribute to deshielding induced by the electron-poor heptazine ring. To confirm the NMR assignments, we performed cross polarization with polarization inversion[30] (CPPI, Figure 2e) and double correlation ^{1}H–^{15}N–^{13}C 2D NMR experiments (Figure 2f). For the CPPI experiment, the lack of decay for N1 (outer heptazine nitrogen) and N2 (central heptazine nitrogen) is consistent with the absence of directly bonded protons, which identifies these nitrogens as the tertiary nitrogens of the heptazine ring. The decay of N3 with a crossover point of ≈0 is consistent with the NH group, while the decay of N4 has a crossover point of ≈–0.5 and is close to the theoretical value of –⅓ for NH_2. For the double correlation experiment, long-distance couplings are observed with the NMR parameters used. Nonetheless, coupling of N4 to both C1 and C2 is consistent with urea at a heptazine terminal. From the elemental analysis (**Table 1**), the C:N atomic ratio of 0.70 for urea-CN_x is consistent with both a 1D polymeric structure (Scheme S1, bottom left, Supporting Information) and the idealized PHI network structure (Scheme S1, bottom right, Supporting Information) with a C:N ratio of <0.706. The near

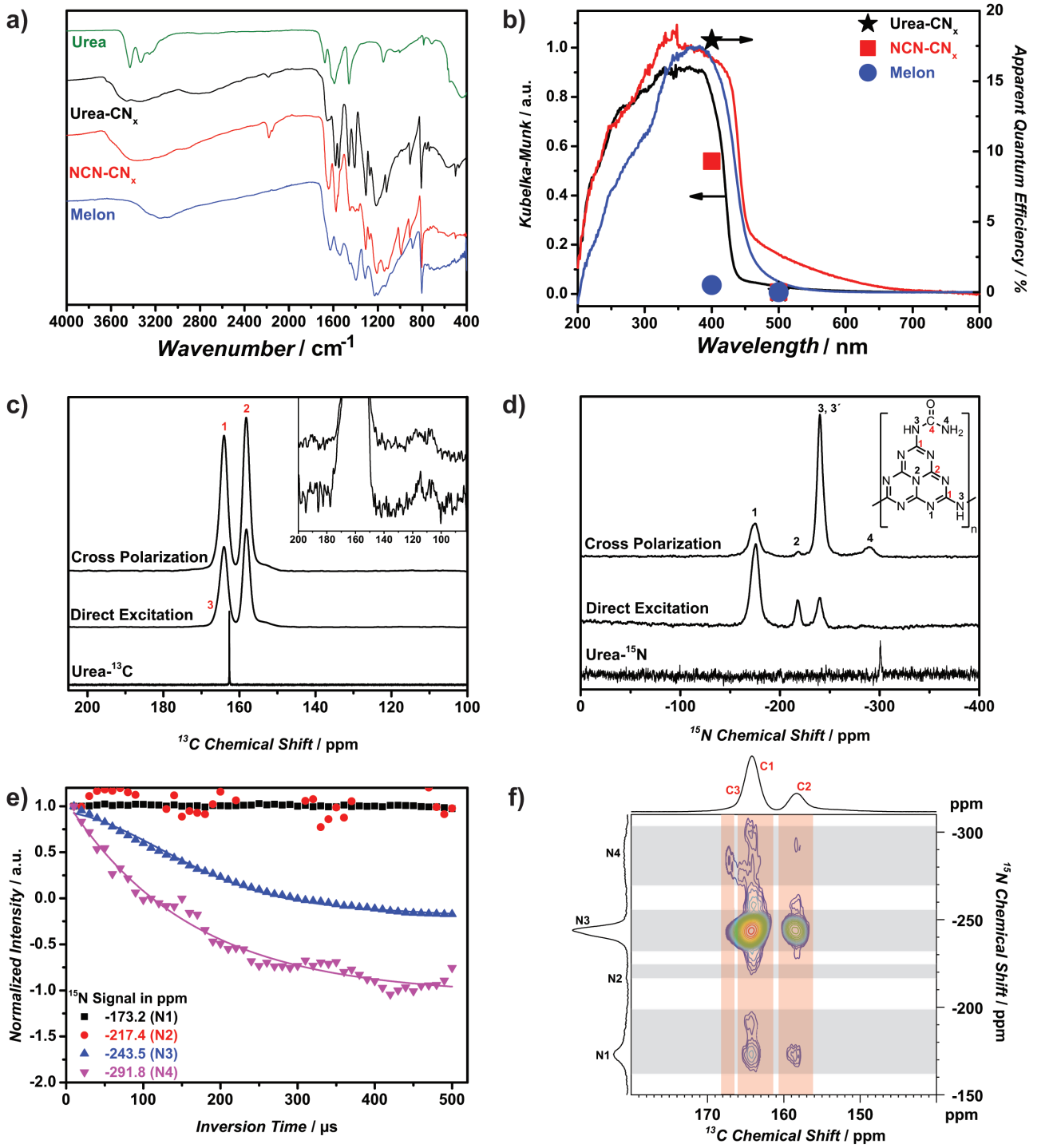

Figure 2. Spectroscopic characterization of urea-CN_x: a) Fourier transform infrared spectroscopy (FTIR); enlarged spectra in the 2400–1400 cm^{-1} range are shown in Figure S2, Supporting Information, b) action spectrum compared to those of NCN-CN_x and melon, c) ^{13}C and d) ^{15}N magic angle spinning solid state NMR (MAS ssNMR) with either ^{1}H cross polarization (CP) or direct excitation; inset of (c) is an enlarged version showing the minute ^{13}C cyanamide signal, while the inset of (d) shows the proposed structure of urea-CN_x and the NMR assignment, e) evolution of signal integrals versus inversion time in the ^{15}N CPPI experiment and estimation of the turning points, f) ^{15}N–^{13}C 2D spectrum of the $^{1}H \rightarrow {}^{15}N$, $^{15}N \rightarrow {}^{13}C$ double cross polarization experiment. Comparisons of the ^{13}C and ^{15}N NMR spectra were made with ^{15}N-enriched urea in D_2O. Deconvolution of the N3 signal in the ^{15}N CP NMR is shown in Figure S2 (Supporting Information).

absence of potassium signifies that the bulk of the compound is not ionic as in NCN-CN_x, although the residual potassium can be associated with the presence of unreacted NCN-CN_x, which may be buried within the polymer and inaccessible to the acid. This unreacted species is discernible by the small FTIR signal at 2180 cm^{-1} (see Figure S2, Supporting Information, for enlarged

Table 1. Elemental analyses and C:N molar ratios of the urea-CN_x, NCN-CN_x, melon, and PHI; all values are weight percentages and uncertainties are the standard deviations of measurement replicates.

	C	N	K	S	C:N molar ratio	C:N molar ratio (th.)
Urea-CN_x	28.8 ± 0.3	48.2 ± 0.2	0.134 ± 0.001	0.017 ± 0.004	0.699 ± 0.007	0.700
NCN-CN_x	26.7 ± 0.0	44.4 ± 0.1	7.54 ± 0.08	0.17 ± 0.11	0.701 ± 0.002	0.700
Melon	35.4 ± 0.1	60.6 ± 0.5	–[a)]	–[a)]	0.681 ± 0.006	0.667[b)]
PHI[c)]	37.4	61.8	–	–	–	0.706

[a)]Not measured; [b)]Assuming infinite 1D heptazine polymer with a unit cell formula $C_6N_9H_3$; [c)]Theoretical values based on a unit cell formula of $C_{12}N_{17}H_3$ based on ref. [12], but without the central melamine.

spectra of this region), the broad signal between 125–102 ppm in the ^{13}C spectrum (Figure 2c inset) and at ≈–280 ppm in the ^{15}N spectrum, corresponding to the NCN moiety in NCN-CN_x.

Characterization of urea-CN_x by transmission and scanning electron microscopy (TEM and SEM), x-ray diffraction (XRD), and sorption analyses (**Figure 3**) shows that this material consists of platelets with lateral dimensions of 40–80 nm. Its nanoscale morphology leads to a comparatively large BET surface area of nearly 65 $m^2\ g^{-1}$ with mainly textural (interparticle) porosity in the nanometer range, which was achieved without employing sacrificial hard templates. The short interlayer spacing of 3.2 Å and structural periodicity of 11 and 8.6 Å are observable in the TEM, XRD, and electron diffraction patterns and are identical to that of NCN-CN_x, indicating that the acid hydrolysis did not affect the general macroscopic structure. Additionally, like NCN-CN_x, urea-CN_x has around 20 wt% water based on its thermogravimetric analysis (Figure S3, Supporting Information). Otherwise, one noticeable difference is the reduced *d*-spacing for urea-CN_x of 8.6 Å, compared to 9.0 Å for NCN-CN_x, a decrease which may be related to tighter packing as the urea group can form hydrogen bonds with neighboring heptazine units. As consistent with this explanation, we observe in the 2D ^{15}N–^{13}C spectrum that the urea NH_2 (N4) couples not only to the urea carbon C3 and the outer heptazine carbon C1, but also couples over longer distance to the inner heptazine carbon C2.

In order to analyze the charge transfer properties of urea-CN_x, steady-state photoluminescence (PL) spectra were

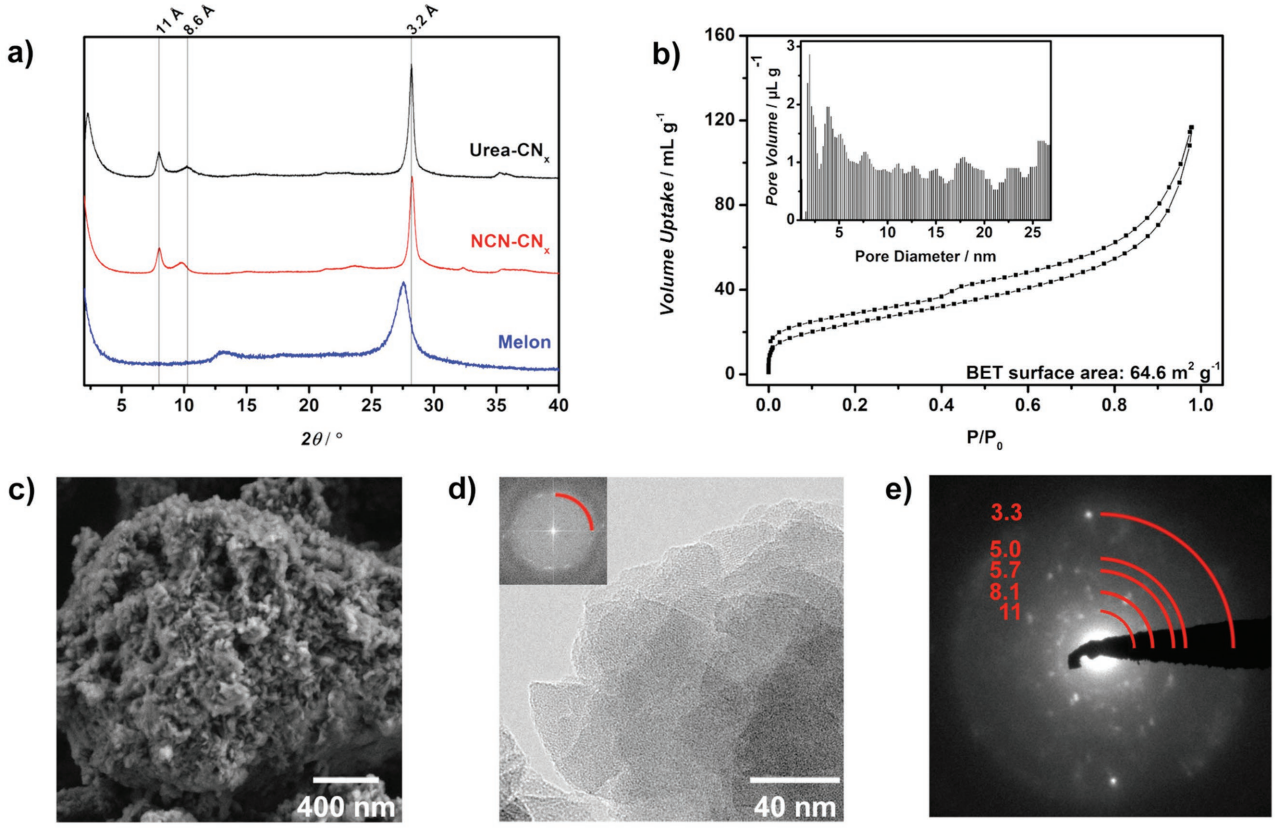

Figure 3. Characterization of urea-CN_x: a) XRD pattern of urea-CN_x compared with those of NCN-CN_x and melon, b) argon sorption isotherm and pore size distribution (inset), c) SEM, d) TEM and its fast Fourier transform (inset), where the red quarter circle shows a *d*-spacing of 10.4 Å, and e) electron diffraction pattern, where the quarter circles show *d*-spacings in Å.

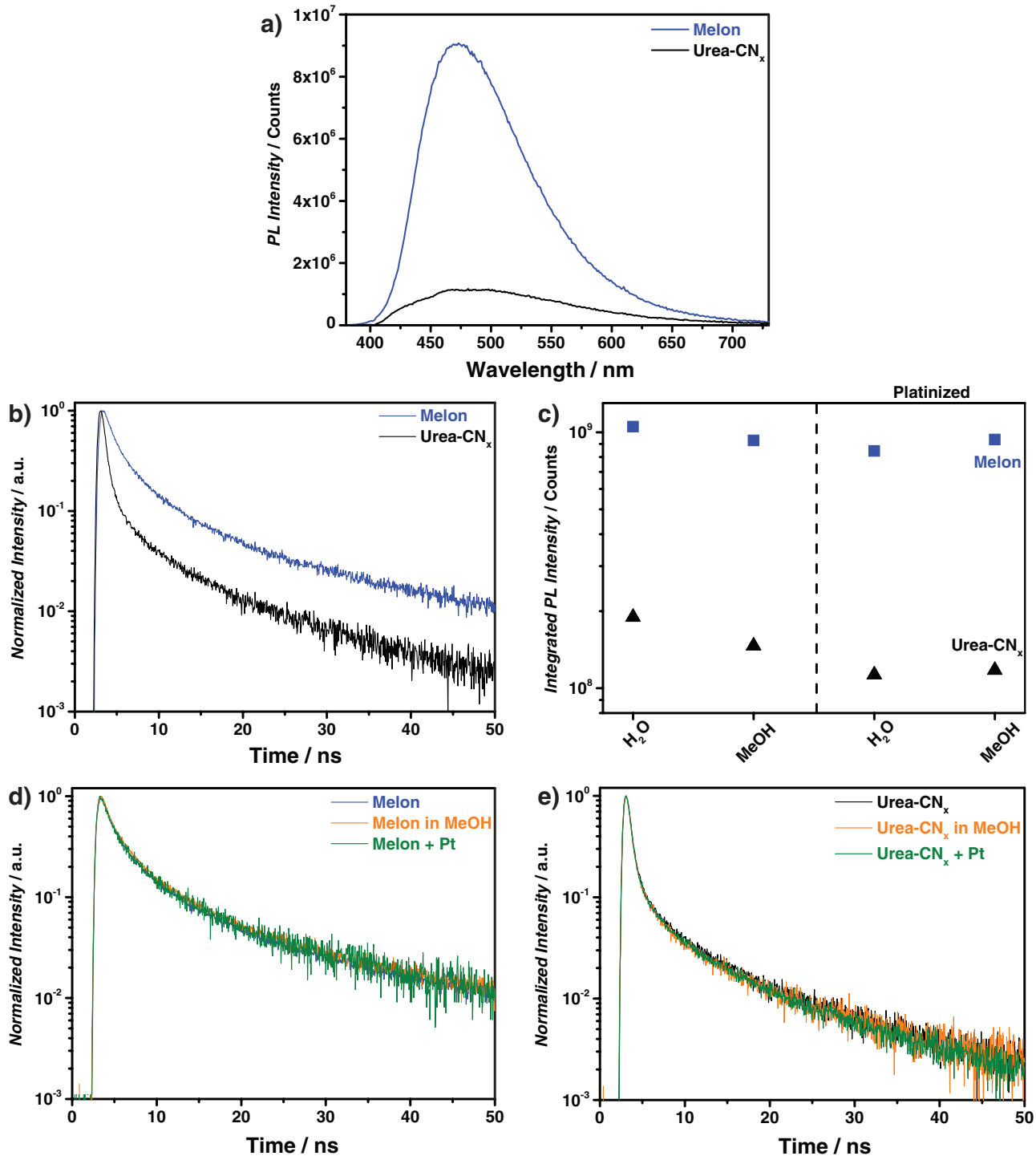

Figure 4. a) PL spectra with excitation at 375 nm of aqueous suspensions of melon and urea-CN_x, b) PL decay curves of melon and urea-CN_x, c) comparison of the PL intensity for melon and urea-CN_x under different environments based on the integral of the PL signal; comparison of PL decay curves of d) melon and e) urea-CN_x in the presence of the electron (Pt) or hole acceptor (MeOH).

acquired for 1 mg mL^{-1} aqueous suspensions of melon and urea-CN_x upon excitation at 375 nm (**Figure 4**a). The latter exhibited reduction of the PL signal by 83% compared to melon. Such inverse relationship between photocatalytic activity and PL intensity is commonly observed in many photocatalysts[31] and is usually understood in terms of a competition for photo-excited charges between the radiative and charge separating channels. The charge transfer pathway leading to hydrogen generation can be considered as an additional or more efficient nonradiative channel, leading to a decrease in luminescence.

The time-resolved PL measurements (Figure 4b) show a much faster PL decay for urea-CN_x ($\tau_{1/e}$ lifetime of 0.77 ns) than for melon ($\tau_{1/e}$ lifetime of 2.4 ns). Taken together with the reduced PL quantum yield of urea-CN_x, they indicate a threefold to fourfold faster nonradiative recombination rate in urea-CN_x than in melon, in agreement with the above interpretation.[32]

Interestingly, as shown in Figure 4c (spectra shown in Figure S4, Supporting Information), the addition of an electron acceptor (decoration with Pt) or a hole acceptor (10 vol% methanol) to either of the two materials results in only very moderate (10%–15%) quenching of the PL; the apparent increases in PL intensity upon addition of methanol to the platinized samples are within experimental error. The corresponding PL decay traces (Figure 4d,e) show no change upon the addition of Pt or methanol, even though the presence of a cocatalyst and a hole scavenger strongly increases the photocatalytic efficiency. These results are unusual since in CdS-based photocatalysts, for example, the decoration with cocatalyst strongly quenches PL and leads to much faster signal decay.[33] This suggests that in the first step the photoexcited charges transfer to the internal site on the polymer, presumably the pendant primary amine and urea moiety on melon and urea-CN_x, respectively. The lack of correlation between the PL decay rate and the presence of Pt means that this initial step is independent (i.e., proceeds on a different time scale) of the subsequent electron transfer to Pt and onward to a proton and does not constitute the limiting step of the hydrogen generation process. Consequently, the difference in photocatalytic efficiency between melon and urea-CN_x possibly arises from different transfer rates from the internal site to the Pt particle (or directly to a proton in case of a nonplatinized system), depending on the coupling between this site and the Pt particle.

To further explore the rationale for the high performance of urea-CN_x, namely the role of the urea moiety and its interaction with the Pt cocatalyst, the spent catalyst with the Pt photodeposited in situ after the 100+ hour photocatalytic experiment was fully characterized (**Figure 5**). The FTIR and ^{13}C NMR spectra and the XRD patterns are essentially identical between the pristine and the spent catalyst, demonstrating chemical and morphological stability of urea-CN_x after the photocatalytic reaction. In the ^{15}N CP ssNMR spectrum, appearance of peak shoulders for N1, N3, and possibly at N4 can be attributed to the presence of the Pt cocatalyst and will be elaborated below. Similarly for the x-ray photoelectron spectra (XPS), the general peak shapes are largely unchanged after the photocatalytic reaction, although small shifts in the binding energies are observed. Briefly, assignment of the deconvoluted XPS signals, based on previous publications, is as follows. The signals for the heptazine sp^2 carbons and nitrogens occur at 288.6 and 399.1 eV, while the sp^3 nitrogen of the bridging 2° amine occurs at 400.8 eV.[34] The C1s signal at 286.5 eV may be assigned to the sp^2 carbon of urea, while the broad signal at 293.6 eV is attributed to potassium associated with the unreacted cyanamide anion from NCN-CN_x. As illustrated in Figure 5, some C and N signals as well as the oxygen signal from urea are shifted to higher binding energy (B.E.), with the oxygen shifting by 0.3 eV, well above the resolution of the XPS. For the in situ deposited Pt, the Pt XPS $4f_{7/2}$ signal can be deconvoluted into Pt^{2+} and Pt^0 species as consistent with observation from others[35] and our previous research.[17] While the B.E. of the Pt^0 species (70.9 eV) is slightly shifted compared to NCN-CN_x (71.1 eV) and melon (71.2 eV), the Pt^{2+} species at 71.9 eV, which has been assigned in the literature to a PtO shell around the metallic Pt,[35] is shifted to lower B.E. by over 0.4 eV compared to NCN-CN_x (72.3 eV) and melon (72.4 eV). Invariance of the N_{1s} signal at 400.8 eV corresponding to the hydrogen bearing 2° amine lent confidence that the aforementioned shifts are not calibration errors. The directions of the shifts—toward higher B.E. for the carbon nitride and lower B.E. for the Pt—are in accord with a metal-support interaction (MSI), specifically the donation of electron density from the carbon nitride to the Pt.[36] Given that both the oxygen and the Pt^{2+} XPS signals are shifted by around the same magnitude but opposite direction, this would suggest that the urea moiety is involved in connecting with the cocatalyst, facilitating charge transfer, and thus leading to the significant increase in photocatalytic hydrogen evolution. These XPS results are in fact consistent with previous adsorption studies, which have found that the adsorption of urea onto a Pt surface is accompanied by charge transfer from the adsorbate to the metal surface.[37]

Characterization by electron microscopy and diffraction (**Figure 6** and Figure S5, Supporting Information) showed not only formation of Pt particles with diameter of 2–4 nm but also that these particles seemingly trace the edge of the platelets. This suggests that the urea-CN_x contained preferential sites for Pt to coordinate to and to subsequently be reductively photodeposited from H_2PtCl_6. In the absence of more element-specific techniques (x-ray absorption spectroscopy (XAS) and electron tomography), our inference consistent with our above ^{15}N NMR and XPS findings as well as literature precedents is that the urea moieties at the periphery are coordinating through the oxygen to the Pt cocatalyst.

As a final indicator, we use electronic structure theory to corroborate the implications derived from the experimental observations above. We note that replicating the precise mechanistic details of the photocatalyst and its operation by first-principles modeling would significantly exceed the capabilities of any first-principles approaches currently available. However, several key open questions that can be addressed relate to how the interaction with the Pt cocatalyst differs between differently functionalized substrates, particularly melon and urea-CN_x. These questions include: (1) the extent of the support/cocatalyst interaction, (2) the moieties involved in the coordination to the Pt cluster, and (3) the potential for electron versus hole transfer to the Pt cluster. Below, we approach these questions using still demanding, yet feasible, ground state density-functional theory (DFT)-based simulations. The findings reported here aim to elucidate the characteristics that improve the electron transfer to the platinum, which based on the above discussions appears to be the rate limiting step. They do not, however, model the inherent carrier dynamics of the carbon nitrides, such as the processes related to charge carrier separation or the percolation of charges inside the carbon nitride as discussed in the PL section.

Specifically, we address questions 1–3 by comparing the electronic structure of two different computational models of the substrate-Pt interaction shown in **Figure 7**: (i) a Pt_{13} cluster adsorbed on a bilayer of melon (Figure 7a,c) and (ii) a Pt_{13}

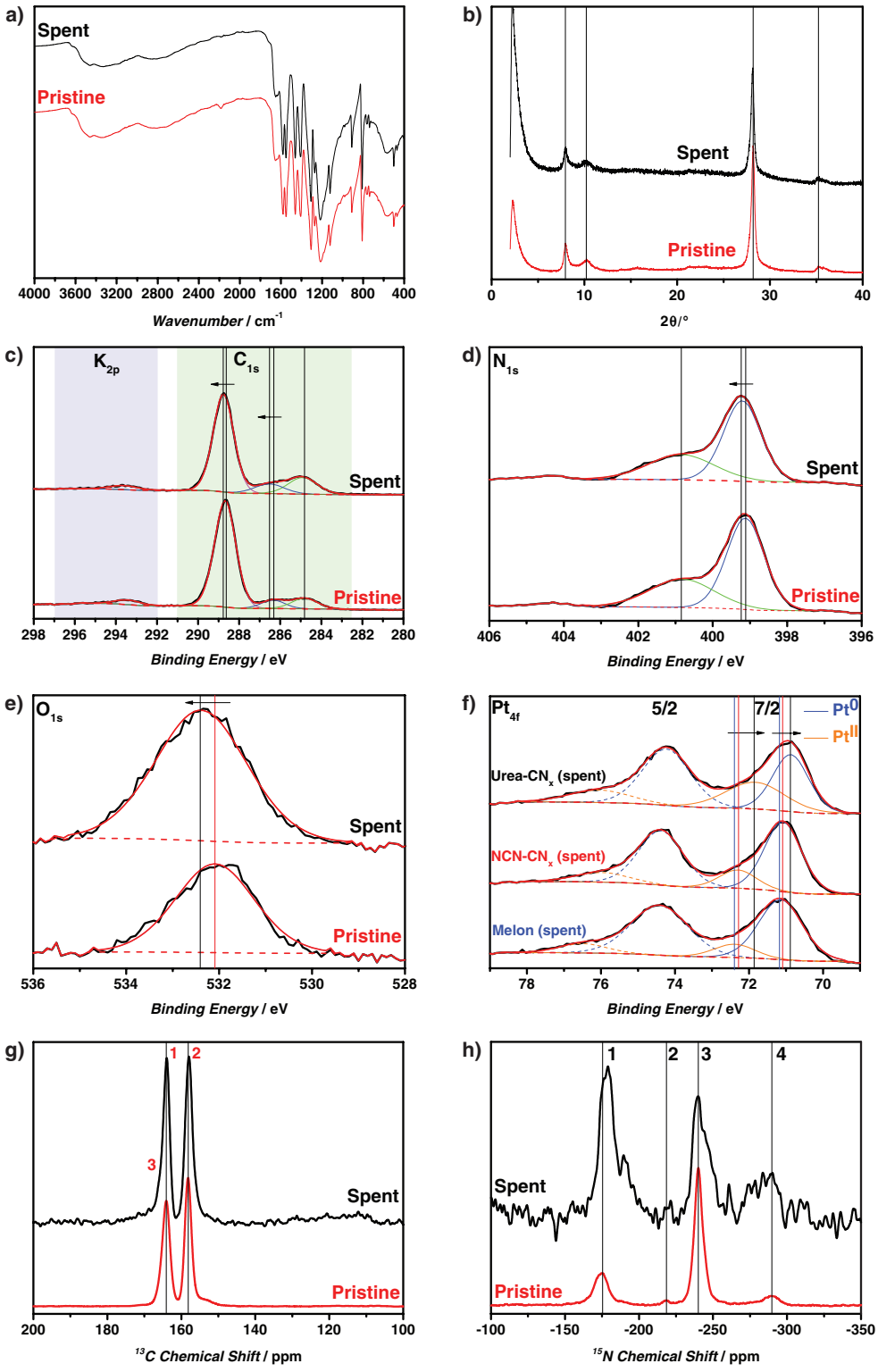

Figure 5. Characterization of the spent photocatalyst compared to the pristine material by: a) FTIR, b) XRD; XPS spectrum referenced to adventitious carbon at 284.8 eV in the c) K_{2p} and C_{1s}, d) N_{1s}, e) O_{1s}, and f) Pt_{4f} regions. For (c)–(e), the black and red hairlines correspond respectively to the spent and pristine urea-CN_x, while for (f) the black, red, and blue hairlines correspond to urea-CN_x, NCN-CN_x, and melon, respectively. For (c)–(e), the direction of the peak(s) shift of the spent compared to the pristine catalyst is indicated by the arrow. For (f), the arrows show the direction of the peak shift going from melon to NCN-CN_x to urea-CN_x. g) ^{13}C direct excitation and h) ^{15}N CP MAS ssNMR. Since only changes in the chemical environments, rather than their quantification, are of interest in the NMR spectra, the spent catalyst with natural isotopic abundance is compared with the pristine one from Figure 2, which has 99% ^{13}C and ^{15}N isotope enrichment.

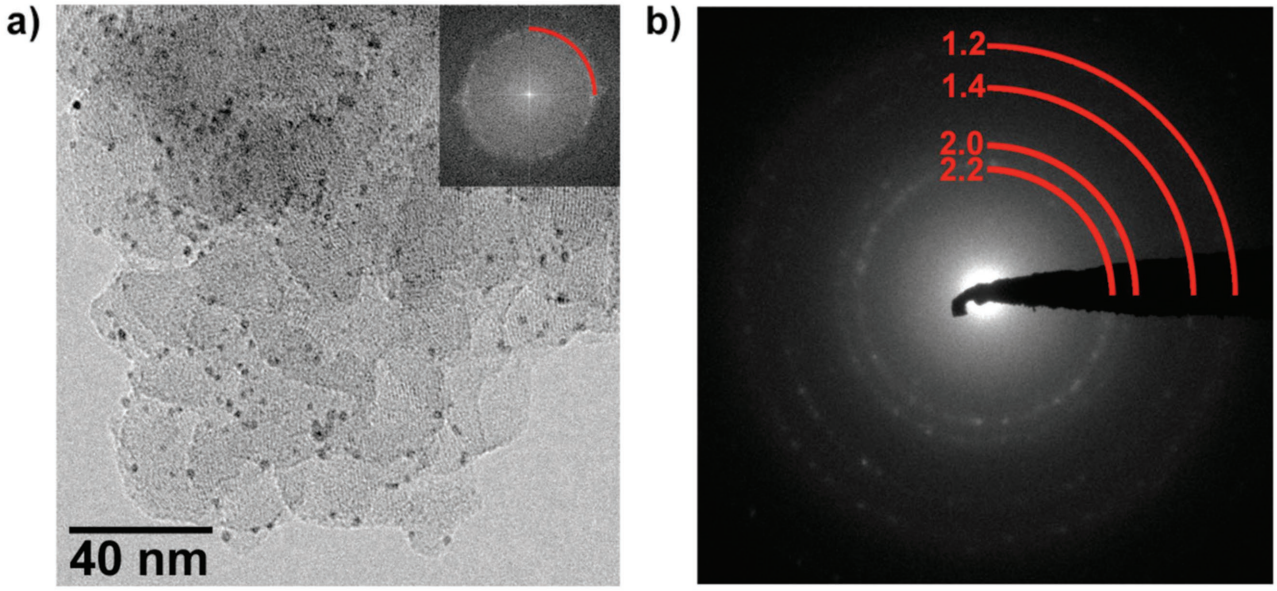

Figure 6. Electron microscopy analyses of the urea-CN_x after 100+ h photocatalysis: a) TEM and the FFT with the quarter circle indicating a *d*-spacing of 11 Å (inset), b) electron diffraction pattern showing the *d*-spacings in Å of Pt.

cluster adsorbed on a conceptual structural model of a bilayer of urea-CN_x (Figure 7b,d). While the structure of melon layers is reasonably well established from past theory and experiment, we do not, at this point, know the precise atomic structure of urea-CN_x planes. In order to facilitate a meaningful comparison between both substrates, we therefore choose a computational structure model for the urea-CN_x structure that allows us to focus specifically on the differences that arise from replacing the NH_2 side chains of melon with the NH-CO-NH_2 side chains of urea-CN_x. The chosen model substrate geometry of urea-CN_x is thus as similar as possible to melon, i.e., a hydrogen-bonded bilayer model of 1D heptazine polymer strands, but with all NH_2 groups replaced by urea moieties (see Scheme S1, bottom left, Supporting Information). Both structure models are realized as periodically repeated supercells. The unit cell dimension perpendicular to the bilayers (*z*-direction) is 40 Å, ensuring a large vacuum region. Additionally, we employ a dipole correction[38] in the *z*-direction to prevent interactions between different periodic images. The periodic images of the adsorbed Pt_{13} clusters are separated by using lateral supercell dimensions of four parallel heptazine strands with six heptazine units along each strand in each layer. For the initial geometry of Pt_{13}, we chose a minimum-energy structure determined by Piotrowski et al.[39] The full bilayer models including the Pt_{13} cluster comprise a total of 877 atoms for melon and 1069 atoms for urea-CN_x. All atomic positions and lateral unit cell parameters were fully relaxed to the nearest local minima of the potential-energy surface. The urea-CN_x model analyzed in Figure 7b,d is the lowest-energy model out of three different cluster-bilayer models that we tested for urea-CN_x, all of which included the attachment of Pt_{13} to O as an important feature. All calculations were performed using the FHI-aims all-electron electronic structure code,[40] "light" settings and the Γ point for Brillouin zone integration, and the Perdew–Burke–Ernzerhof (PBE)[41] density functional together with the Tkatchenko–Scheffler pairwise van der Waals dispersion correction[42] (PBE+vdW).

In Figure 7a,b, we show the element-resolved partial densities of states of Pt_{13} adsorbed at the melon bilayer versus at the urea-CN_x bilayer, respectively. We note that, without adsorbed Pt_{13} and in DFT-PBE, the melon bilayer would have a HOMO–LUMO (highest occupied and lowest unoccupied molecular orbital) gap of 2.53 eV, whereas the Pt-free urea-CN_x bilayer would have a smaller HOMO–LUMO gap of 2.25 eV; these values are consistent with the C—N band edges inferred from Figures 7a,b when Pt_{13} is present. Insets in both figures show the fully relaxed local Pt_{13} adsorption geometry at either substrate. Furthermore, the complete model geometries used for melon and urea-CN_x are also shown in Figure 7c,d, respectively, together with the orbital densities of two particular hybridized states close to (at or just below) the substrate LUMO levels (see below). Coming to the geometries first (provided in the NoMaD repository; link given in the experimental section), the melon bilayer, which has strong hydrogen bonding within the plane, shows comparatively little structural rearrangement as a result of Pt_{13} adsorption. Here, the Pt_{13} cluster shifts to connect to one of the NH_2 functionalities, which is slightly pulled out of the plane. In contrast, the urea-CN_x bilayer model displays a substantial rearrangement of its atomic positions. In line with the experimental conclusions, there is a direct attachment of Pt_{13} to the O functionality of urea as well as a connection to several of the N atoms of different adjacent heptazine rings. We also estimated the overall charge transfer from the substrates to the neutral Pt_{13} cluster by Hirshfeld[43] atoms-in-molecules partitioning schemes. Both schemes indicate practically no charge transfer from melon to Pt_{13} (Mulliken: –0.18 e, Hirshfeld: 0.0 e) and a small transfer of electrons to Pt_{13} (Mulliken: –0.571 e, Hirshfeld: –0.15 e) for our particular urea-CN_x-Pt_{13} model.

We next turn to a closer analysis of the hybridization of Pt_{13} states with the near-edge carrier states of the substrates. Since

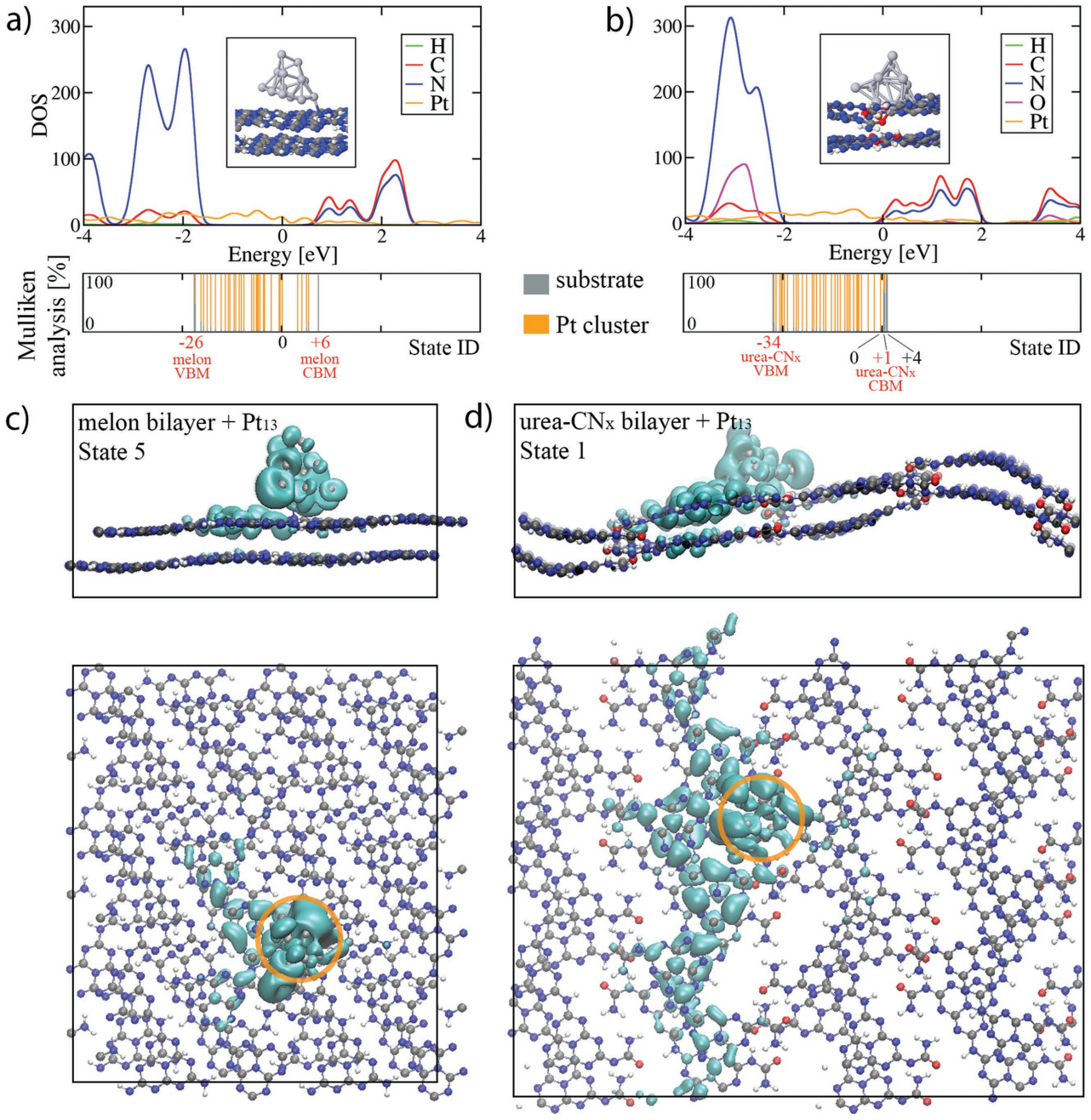

Figure 7. First-principles model of the interaction of melon versus urea-CN_x with a Pt_{13} cluster. H: white; C: gray; N: blue; O: red; Pt: silver. a) Element-resolved smoothed partial density of states of the melon bilayer + Pt_{13} cluster model. Inset: Pt_{13} attachment via NH_2 side group. b) Element-resolved smoothed partial density of states of the urea-CN_x bilayer + Pt_{13} cluster model used in this work. Inset: Pt_{13} attachment via O. The lower panels in (a) and (b) show Mulliken decompositions of selected individual levels inside the melon/urea-CN_x model HOMO–LUMO gaps. Two-colored bars, gray and orange, mark the bilayer substrate versus Pt_{13} cluster fractions of each state. Numbers on the *x* axes index the selected states in order of their single-particle energy, with zero indicating the highest state with a fractional occupation of 0.5 or above. c) Side and top views of the orbital density of the partially hybridized state (state ID 5 in lower panel of (a)) located at 0.20 eV below the LUMO of the melon substrate (state ID 6 in lower panel of (a)). d) Top and side views of the orbital density of the strongly hybridized state (state ID 1 in lower panel of (b)) with contributions from Pt_{13} and from the urea-CN_x substrate LUMO. Orange rings in the top views indicate the location of the Pt_{13} cluster.

the Pt_{13} cluster is finite, the energies of its states found in the band gaps of melon and urea-CN_x are discrete. We can therefore analyze the character of each state near and in-between the substrate band edges by performing a Mulliken decomposition into contributions from the Pt_{13} cluster and contributions from the substrates. The result of the state-resolved Mulliken analysis is shown in the bottom panels of Figures 7a,c. For comparison, we also visualize the orbitals associated with all states close to or

in-between the band edges of Pt_{13}-melon and of Pt_{13}-urea-CN_x in Figures S8–S13 (Supporting Information). The individual states are labeled by consecutive integer numbers. The number zero indicates the state closest to the Fermi level, here taken to be the highest-energy state with an electronic occupation greater than 0.5. Negative labels indicate filled states and positive numbers indicate empty states. Based on the Mulliken analyses, we assign the state labeled "–26" in the lower panel of Figure 7a to the valence band maximum (VBM/HOMO) of melon. The state labeled "6" in Figure 7a is assigned to the conduction band minimum (CBM/LUMO) of melon. Similarly, the states labeled "–34" and "1" in Figure 7b are assigned as the VBM/HOMO and CBM/LUMO of the urea-CN_x bilayer, respectively. However, states 2–4 are very close to state 1 in energy and are predominantly CN_x derived as well. They are thus likely to be closely associated with the CBM/LUMO as well.

The discrete states in the band gaps of melon and of urea-CN_x are almost purely Pt_{13} derived. However, a few states near the band edges show a greater degree of hybridization. Let us first analyze the electron-like states near the CBMs/LUMOs. For melon-Pt_{13}, a particular state of interest is the partially hybridized state 5, just 0.2 eV below the apparent LUMO of melon. The orbital density of this state is shown in Figure 7c. State 5 is strongly localized near the Pt_{13} cluster but extends to a few heptazine units of the substrate. This or similar hybridized states associated with the NH_2 moieties of melon could well serve as the states that facilitate electron transfer to the Pt cocatalyst in general. The case of urea-CN_x is strikingly different in that the states derived from its LUMO (just above the highest occupied level of the Pt cluster) appear to be significantly more hybridized with the Pt states. As an example, Figure 7d shows the orbital density for state 1 in the lower panel of Figure 7b, which is much more extended along the strands near the Pt cluster than is the case for state 5 of Figure 7c (melon). Assuming that these hybridized states can be viewed as indicative of electron transfer pathways to the Pt cluster, the comparison indeed suggests that the electron transfer could be more effective in the presence of urea functionalities than for the unmodified melon.

Regarding the states near the substrate VBMs/HOMOs, we observe that state –26, the HOMO of melon, is not appreciably hybridized with the Pt_{13} cluster, but several other states just above it show some hybridization. In contrast, our urea-CN_x-Pt_{13} model shows no significant hybridization of the Pt-derived states with the HOMO, i.e., with the potential hole-like states.

In summary, the results from our DFT–PBE+vdW model calculations are supportive of key observations relating to the Pt-substrate interaction, specifically of an overall stronger metal-support interaction for urea-CN_x, facilitated via O moieties and of a stronger hybridization of the electron-like states of urea-CN_x with Pt-derived states. The latter could be indicative of more facile electron transfer pathways available in urea-CN_x than in the archetype melon.

Collectively, our results above may provide a retrodictive explanation to the observation that melon prepared from urea, rather than from dicyandiamide or melamine, performed better photocatalytically.[20] The literature rationales for this observation have been attributed to increased surface area[20a] or increased condensation in the carbon nitride.[20b] While the former certainly contributes to the increased activity, Martin et al. have argued it does not sufficiently account for the vast improvement observed.[20b] Indeed, our results infer that the higher activity observed in melon prepared from urea (henceforth notated as melon (urea)) as compared to that from melamine is attributable to residual functional groups, namely the urea moiety, from the incomplete cyclization and condensation of urea to heptazine via dicyandiamide and melamine. For example, oxygen can be incorporated from ureidomelamine,[44] an impurity in melamine, or from trace water and oxygen in the synthesis atmosphere. To verify our retrodiction, we prepared a sample of melon from urea for comparison of the characterization results (**Figure 8**). As predicted, a small but nonetheless discernible urea signal is observed in the ^1H–^{15}N CP NMR at around –290 ppm for melon (urea), which is absent for melon, and coincides with the urea NH_2 signal (N4) for urea-CN_x. Furthermore, the spectra for melon (urea) resemble urea-CN_x more than those for melon, particularly the apparent downfield shifts for the NMR signals of the heptazine core (N1 and C2; N3 to a lesser extent).

In agreement with previous literature, we found that melon (urea), despite absorbing less in the visible region as evident in their UV–vis spectra (Figure 8c), performs better for photocatalytic hydrogen evolution than melon: 4.4 versus 1.8 μmol h^{-1} averaged over the first 8 h under AM1.5 irradiation and 4.7% versus 0.5% AQE at 400 nm. We emphasize that these values are still much lower than that of urea-CN_x or NCN-CN_x (56.2 and 24.7 μmol h^{-1}, respectively). Through additional characterizations, we rule out as the principal factors for the outperformance of urea-CN_x the variations in (1) BET surface area, (2) dispersibility in water as measured by zeta potential, (3) Pt loading, and (4) Pt size, morphology, and distribution (see the Supporting Information for detailed discussions). From this, we deduce that efficient charge transfer mediated by the platinum/urea-CN_x interaction seems to be a key determinant for its high activity. This work thus highlights the success of our "defect engineering" strategy by the rational insertion of the activity-promoting functional group into the carbon nitride backbone.

3. Conclusion

Treating melon in a KSCN melt followed by acid hydrolysis yielded a carbon nitride polymer decorated with the urea functional group. This urea-CN_x exhibited one of the highest photocatalytic activities for hydrogen evolution reported for carbon nitrides thus far, with rates over twice that of the NCN-CN_x and over 28 times that of melon under simulated sunlight using methanol as the electron donor. Likewise, the apparent quantum efficiency at 400 nm of this urea-CN_x (17.9%) is nearly twice that of NCN-CN_x (9.3%) and nearly 36 times that of melon (0.5%). We attribute this large improvement in activity primarily to the rational insertion of the urea moiety which appears to be the preferential docking site for the platinum cocatalyst and to facilitate transfer of photogenerated charges into the hydrogen evolving centers, based on results from TEM, XPS, and computational modeling. Following these results, we suggest a retrodictive explanation to the better photocatalytic performance of

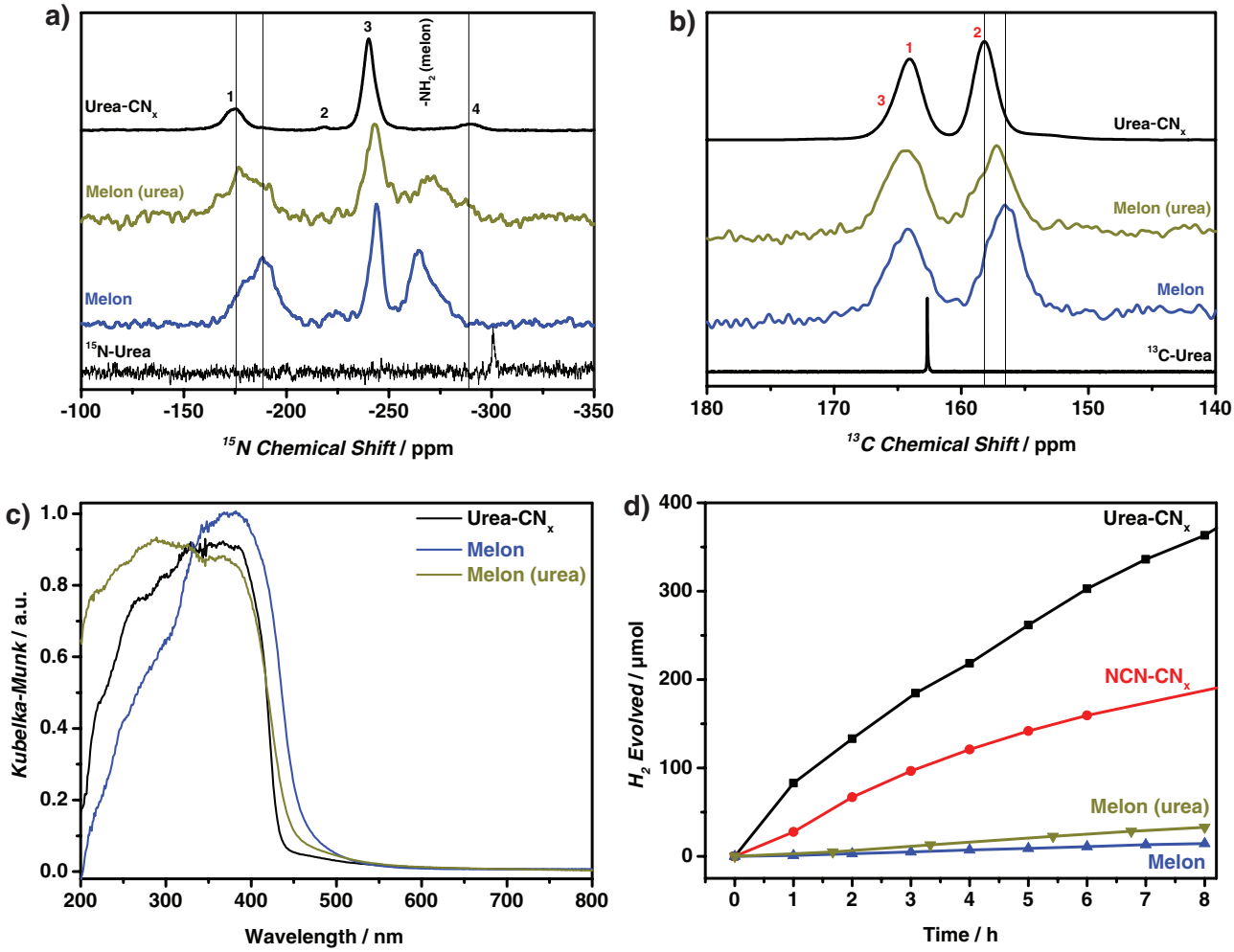

Figure 8. Comparison of urea-CN$_x$ and melon prepared from urea and melamine: a) ^{15}N CP and b) ^{13}C direct excitation NMR, with lines drawn to illustrate how the spectra for melon (urea) resemble urea-CN$_x$ as compared to melon. Identical to Figure 2c,d, the black and red numbers are assignment of the ^{15}N and ^{13}C signals, respectively, to the proposed local structure of urea-CN$_x$ (Figure 2d inset). Note that both melon and melon (urea) are not isotope enriched. c) Diffuse reflectance UV–vis spectra and d) photocatalytic hydrogen evolution from methanol solution under AM1.5 irradiation (right).

melon prepared from urea compared to those from melamine and dicyandiamide. This rationale was subsequently supported by experimental evidence and for the first time sheds light on the role and nature of oxygen-containing catalytically relevant sites in carbon nitride photocatalysts. Specifically, residual urea groups from incomplete heptazine cyclization and decomposition were found in melon prepared from urea, which are not in detectable abundance in the melon samples from melamine. The strategy presented herein can be considered as an example of "functional defect design" or engineering of catalytically relevant sites, where we deliberately inserted the photocatalytically relevant defect. The vast increase in activity of this engineered sample attests to the success of this strategy which, based on extensive characterization of the urea-CN$_x$, appears to be an even more promising research direction for improving photocatalytic activity than redshifting the absorption onset or increasing the surface area, as it can subsequently be combined with all of these latter strategies. Further exploration of mechanistic aspects as well as exploring other defects native or non-native to melon may thus provide the design criteria for highly efficient heptazine-based photocatalysts for not only the hydrogen evolution reaction but also other photoreactions demonstrated to be feasible for this material such as water oxidation, CO_2 reduction, and organic transformations.

4. Experimental Section

Details of the syntheses and characterization techniques are provided in the Supporting Information. Computational results are provided in the NoMaD repository under the link http://dx.doi.org/10.17172/NOMAD/2016.11.14-1; computationally calculated structures are also uploaded in the Supporting Information as cif.

Supporting Information

Supporting Information is available from the Wiley Online Library or from the author.

Acknowledgements

V.W.L. gratefully acknowledges a postdoctoral scholarship from the Max Planck Society. This work was supported by the Deutsche Forschungsgemeinschaft (project LO1801/1-1), the Max Planck Society, the cluster of excellence Nanosystems Initiative Munich (NIM), and the Center for Nanoscience (CeNS), and the Bavarian State Ministry of Science, Research, and Arts through the grant "Solar Technologies go Hybrid (SolTech)." Support from a seed grant by the Duke University Energy Initiative is gratefully acknowledged. The authors would like to thank Marie-Luise Schreiber for the elemental analyses, Dr. Mitsuharu Konuma for the XPS analyses, and Olaf Alberto von Mankowski for the argon sorption measurements. The acknowledgements were updated on June 21, 2017. The initial of the middle name of the author Jacek Stolarczyk was also added at that time.

Received: October 12, 2016
Revised: December 7, 2016
Published online: January 27, 2017

[1] J. Xing, W. Q. Fang, H. J. Zhao, H. G. Yang, *Chem. – Asian J.* **2012**, *7*, 642.
[2] A. Fujishima, K. Honda, *Nature* **1972**, *238*, 37.
[3] a) B. V. Lotsch, M. Döblinger, J. Sehnert, L. Seyfarth, J. Senker, O. Oeckler, W. Schnick, *Chem. – Eur. J.* **2007**, *13*, 4969; b) K. Maeda, X. Wang, Y. Nishihara, D. Lu, M. Antonietti, K. Domen, *J. Phys. Chem. C* **2009**, *113*, 4940; c) X. Wang, K. Maeda, A. Thomas, K. Takanabe, G. Xin, J. M. Carlsson, K. Domen, M. Antonietti, *Nat. Mater.* **2009**, *8*, 76; d) S. Cao, J. Yu, *J. Phys. Chem. Lett.* **2014**, *5*, 2101; e) J. Liu, H. Wang, M. Antonietti, *Chem. Soc. Rev.* **2016**, *45*, 2308.
[4] a) L. Seyfarth, J. Seyfarth, B. V. Lotsch, W. Schnick, J. Senker, *Phys. Chem. Chem. Phys.* **2010**, *12*, 2227; b) T. Tyborski, C. Merschjann, S. Orthmann, F. Yang, M.-C. Lux-Steiner, T. Schedel-Niedrig, *J. Phys.: Condens. Matter* **2013**, *25*, 395402; c) F. Fina, S. K. Callear, G. M. Carins, J. T. S. Irvine, *Chem. Mater.* **2015**, *27*, 2612.
[5] a) D. M. Teter, R. J. Hemley, *Science* **1996**, *271*, 53; b) E. Kroke, M. Schwarz, E. Horath-Bordon, P. Kroll, B. Noll, A. D. Norman, *New J. Chem.* **2002**, *26*, 508.
[6] M. Döblinger, B. V. Lotsch, J. Wack, J. Thun, J. Senker, W. Schnick, *Chem. Commun.* **2009**, 1541.
[7] a) B. V. Lotsch, W. Schnick, *Chem. Mater.* **2006**, *18*, 1891; b) A. Schwarzer, T. Saplinova, E. Kroke, *Coord. Chem. Rev.* **2013**, *257*, 2032; c) B. V. Lotsch, W. Schnick, *New J. Chem.* **2004**, *28*, 1129.
[8] C. Butchosa, P. Guiglion, M. A. Zwijnenburg, *J. Phys. Chem. C* **2014**, *118*, 24833.
[9] a) G. Liu, P. Niu, C. Sun, S. C. Smith, Z. Chen, G. Q. M. Lu, H.-M. Cheng, *J. Am. Chem. Soc.* **2010**, *132*, 11642; b) Y. Wang, Y. Di, M. Antonietti, H. Li, X. Chen, X. Wang, *Chem. Mater.* **2010**, *22*, 5119; c) J. Zhang, X. Chen, K. Takanabe, K. Maeda, K. Domen, J. D. Epping, X. Fu, M. Antonietti, X. Wang, *Angew. Chem., Int. Ed.* **2010**, *49*, 441; d) Y. Zhang, T. Mori, J. Ye, M. Antonietti, *J. Am. Chem. Soc.* **2010**, *132*, 6294; e) J. Zhang, G. Zhang, X. Chen, S. Lin, L. Möhlmann, G. Dołęga, G. Lipner, M. Antonietti, S. Blechert, X. Wang, *Angew. Chem., Int. Ed.* **2012**, *51*, 3183; f) Z. Lin, X. Wang, *Angew. Chem., Int. Ed.* **2013**, *52*, 1735; g) K. Schwinghammer, B. Tuffy, M. B. Mesch, E. Wirnhier, C. Martineau, F. Taulelle, W. Schnick, J. Senker, B. V. Lotsch, *Angew. Chem., Int. Ed.* **2013**, *52*, 2435.
[10] a) X. Chen, Y.-S. Jun, K. Takanabe, K. Maeda, K. Domen, X. Fu, M. Antonietti, X. Wang, *Chem. Mater.* **2009**, *21*, 4093; b) P. Niu, L. Zhang, G. Liu, H.-M. Cheng, *Adv. Funct. Mater.* **2012**, *22*, 2763; c) J. Sun, J. Zhang, M. Zhang, M. Antonietti, X. Fu, X. Wang, *Nat. Commun.* **2012**, *3*, 1139; d) X. Wang, K. Maeda, X. Chen, K. Takanabe, K. Domen, Y. Hou, X. Fu, M. Antonietti, *J. Am. Chem. Soc.* **2009**, *131*, 1680.
[11] Z. Zhao, Y. Sun, F. Dong, *Nanoscale* **2015**, *7*, 15.
[12] A. Vojvodic, J. K. Nørskov, *Natl. Sci. Rev.* **2015**, *2*, 140.
[13] P. V. Kamat, *J. Phys. Chem. Lett.* **2012**, *3*, 663.
[14] C. Harris, P. V. Kamat, *ACS Nano* **2010**, *4*, 7321.
[15] a) J. Dong, M. Wang, X. Li, L. Chen, Y. He, L. Sun, *ChemSusChem* **2012**, *5*, 2133; b) S.-W. Cao, X.-F. Liu, Y.-P. Yuan, Z.-Y. Zhang, J. Fang, S. C. J. Loo, J. Barber, T. C. Sum, C. Xue, *Phys. Chem. Chem. Phys.* **2013**, *15*, 18363; c) J. Hong, Y. Wang, Y. Wang, W. Zhang, R. Xu, *ChemSusChem* **2013**, *6*, 2263; d) S.-W. Cao, Y.-P. Yuan, J. Barber, S. C. J. Loo, C. Xue, *Appl. Surf. Sci.* **2014**, *319*, 344; e) C. A. Caputo, M. A. Gross, V. W. Lau, C. Cavazza, B. V. Lotsch, E. Reisner, *Angew. Chem., Int. Ed.* **2014**, *53*, 11538; f) H. Kasap, C. A. Caputo, B. C. M. Martindale, R. Godin, V. W.-H. Lau, B. V. Lotsch, J. R. Durrant, E. Reisner, *J. Am. Chem. Soc.* **2016**, *138*, 9183.
[16] V. W.-h. Lau, M. B. Mesch, V. Duppel, V. Blum, J. Senker, B. V. Lotsch, *J. Am. Chem. Soc.* **2015**, *137*, 1064.
[17] V. W.-h. Lau, I. Moudrakovski, T. Botari, S. Weinberger, M. B. Mesch, V. Duppel, J. Senker, V. Blum, B. V. Lotsch, *Nat. Commun.* **2016**, *7*, 12165.
[18] Y. Wang, X. Wang, M. Antonietti, *Angew. Chem., Int. Ed.* **2012**, *51*, 68.
[19] a) T. Güthner, B. Mertschenk, "Cyanamides", *Ullmann's Encyclopedia of Industrial Chemistry*, Electronic Release, Wiley-VCH, Weinheim **2006**; b) M. L. Kilpatrick, *J. Am. Chem. Soc.* **1947**, *69*, 40.
[20] a) Y. Zhang, J. Liu, G. Wu, W. Chen, *Nanoscale* **2012**, *4*, 5300; b) D. J. Martin, K. Qiu, S. A. Shevlin, A. D. Handoko, X. Chen, Z. Guo, J. Tang, *Angew. Chem.* **2014**, *53*, 9240.
[21] a) J. Liu, Y. Liu, N. Liu, Y. Han, X. Zhang, H. Huang, Y. Lifshitz, S.-T. Lee, J. Zhong, Z. Kang, *Science* **2015**, *347*, 970; b) G. Zhang, Z.-A. Lan, L. Lin, S. Lin, X. Wang, *Chem. Sci.* **2016**, *7*, 3062.
[22] T. Maschmeyer, M. Che, *Angew. Chem., Int. Ed.* **2010**, *49*, 1536.
[23] a) A. Salinaro, A. V. Emeline, J. Zhao, H. Hidaka, V. K. Ryabchuk, N. Serpone, *Pure Appl. Chem.* **1999**, *71*, 321; b) N. Serpone, A. Salinaro, *Pure Appl. Chem.* **1999**, *71*, 303.
[24] H. Kisch, D. Bahnemann, *J. Phys. Chem. Lett.* **2015**, *6*, 1907.
[25] M. J. Berr, P. Wagner, S. Fischbach, A. Vaneski, J. Schneider, A. S. Susha, A. L. Rogach, F. Jäckel, J. Feldmann, *Appl. Phys. Lett.* **2012**, *100*, 223903.
[26] S. Horikoshi, N. Watanabe, M. Mukae, H. Hidaka, N. Serpone, *New J. Chem.* **2001**, *25*, 999.
[27] F. Guzman, S. S. C. Chuang, C. Yang, *Ind. Eng. Chem. Res.* **2013**, *52*, 61.
[28] B. Jürgens, E. Irran, J. Senker, P. Kroll, H. Müller, W. Schnick, *J. Am. Chem. Soc.* **2003**, *125*, 10288.
[29] T. Komatsu, *J. Mater. Chem.* **2001**, *11*, 799.
[30] C. Gervais, F. Babonneau, J. Maquet, C. Bonhomme, D. Massiot, E. Framery, M. Vaultier, *Magn. Reson. Chem.* **1998**, *36*, 407.
[31] M. Shalom, S. Inal, C. Fettkenhauer, D. Neher, M. Antonietti, *J. Am. Chem. Soc.* **2013**, *135*, 7118.
[32] a) D. Hollmann, M. Karnahl, S. Tschierlei, K. Kailasam, M. Schneider, J. Radnik, K. Grabow, U. Bentrup, H. Junge, M. Beller, S. Lochbrunner, A. Thomas, A. Brückner, *Chem. Mater.* **2014**, *26*, 1727; b) H. Zhang, A. Yu, *J. Phys. Chem. C* **2014**, *118*, 11628.
[33] a) K. Wu, T. Lian, *Chem. Soc. Rev.* **2016**, *45*, 3781; b) T. Simon, N. Bouchonville, M. J. Berr, A. Vaneski, A. Adrović, D. Volbers, R. Wyrwich, M. Döblinger, A. S. Susha, A. L. Rogach, F. Jäckel, J. K. Stolarczyk, J. Feldmann, *Nat. Mater.* **2014**, *13*, 1013.
[34] A. Thomas, A. Fischer, F. Goettmann, M. Antonietti, J.-O. Müller, R. Schlögl, J. M. Carlsson, *J. Mater. Chem.* **2008**, *18*, 4893.
[35] F. Fina, H. Ménard, J. T. S. Irvine, *Phys. Chem. Chem. Phys.* **2015**, *17*, 13929.

[36] a) P. Bera, K. R. Priolkar, A. Gayen, P. R. Sarode, M. S. Hegde, S. Emura, R. Kumashiro, V. Jayaram, G. N. Subbanna, *Chem. Mater.* **2003**, *15*, 2049; b) F. Zhang, J. Chen, X. Zhang, W. Gao, R. Jin, N. Guan, Y. Li, *Langmuir* **2004**, *20*, 9329; c) Y. Nagai, T. Hirabayashi, K. Dohmae, N. Takagi, T. Minami, H. Shinjoh, S. Matsumoto, *J. Catal.* **2006**, *242*, 103; d) A. Lewera, L. Timperman, A. Roguska, N. Alonso-Vante, *J. Phys. Chem. C* **2011**, *115*, 20153; e) N. G. Akalework, C.-J. Pan, W.-N. Su, J. Rick, M.-C. Tsai, J.-F. Lee, J.-M. Lin, L.-D. Tsaic, B.-J. Hwang, *J. Mater. Chem.* **2012**, *22*, 20977.
[37] a) V. Climent, A. Rodes, R. Albalat, J. Claret, J. M. Feliu, A. Aldaz, *Langmuir* **2001**, *17*, 8260; b) M. García-Hernández, U. Birkenheuer, A. Hu, F. Illas, N. Rösch, *Surf. Sci.* **2001**, *471*, 151.
[38] J. Neugebauer, M. Scheffler, *Phys. Rev. B* **1992**, *46*, 16067.
[39] M. J. Piotrowski, P. Piquini, J. L. F. Da Silva, *Phys. Rev. B* **2010**, *81*, 155446.
[40] a) V. Blum, R. Gehrke, F. Hanke, P. Havu, V. Havu, X. Ren, K. Reuter, M. Scheffler, *Comput. Phys. Commun.* **2009**, *180*, 2175; b) V. Havu, V. Blum, P. Havu, M. Scheffler, *J. Comput. Phys.* **2009**, *228*, 8367; c) F. Knuth, C. Carbogno, V. Atalla, V. Blum, M. Scheffler, *Comput. Phys. Commun.* **2015**, *190*, 33; d) A. Marek, V. Blum, R. Johanni, V. Havu, B. Lang, T. Auckenthaler, A. Heinecke, H.-J. Bungartz, H. Lederer, *J. Phys.: Condens. Matter* **2014**, *26*, 213201.
[41] J. P. Perdew, K. Burke, M. Ernzerhof, *Phys. Rev. Lett.* **1996**, *77*, 3865.
[42] A. Tkatchenko, M. Scheffler, *Phys. Rev. Lett.* **2009**, *102*, 073005.
[43] F. L. Hirshfeld, *Theor. Chim. Acta* **1977**, *44*, 129.
[44] M. Himmelsbach, T. D. T. Vo, *Electrophoresis* **2014**, *35*, 1362.